
Can a single neuron learn quantiles?

Edgardo Solano-Carrillo

German Aerospace Center (DLR)
Institute for the Protection of Maritime Infrastructures
Bremerhaven - Germany
Edgardo.SolanoCarrillo@dlr.de

Abstract

A novel non-parametric quantile estimation method for continuous random variables is introduced, based on a minimal neural network architecture consisting of a single unit. Its advantage over estimations from ranking the order statistics is shown, specifically for small sample size. In a regression context, the method can be used to quantify predictive uncertainty under the split conformal prediction setting, where prediction intervals are estimated from the residuals of a pre-trained model on a held-out validation set to quantify the uncertainty in future predictions. Benchmarking experiments demonstrate that the method is competitive in quality and coverage with state-of-the-art solutions, with the added benefit of being more computationally efficient.

1 Introduction

Estimating how uncertain artificial intelligence systems are of their predictions is crucial for their safe applications (Varshney & Alemzadeh, 2016; Amodei et al., 2016). Quantifying uncertainty is then as important as designing good predictive models. It is an open problem, in part due to its ambiguous character: if predictions are interpreted as subjective opinions, evidence-based theory (Sensoy et al., 2018; Josang et al., 2018; Shi et al., 2020) typically measures uncertainty in entropic terms. On the other hand, if uncertainty is understood as a synonym for the variability of the predictive distribution, prediction intervals (Khosravi et al., 2011a) best summarize this in quantile terms.

Prediction intervals express uncertainty in terms of *confidence* probabilities, of which humans have a natural cognitive intuition (Cosmides & Tooby, 1996; Juanchich & Miroslav, 2020) of guidance for decision making. As such, their use to quantify uncertainty is standardized across a wide variety of safety-critical regression applications, including medicine (IntHout et al., 2016), economics (Chudý M. et al., 2020), finance (Huang & Hsu, 2020); as well as in the forecasting of electrical load (Quan et al., 2014), solar energy (Galván et al., 2017), gas flow (Sun et al., 2017), wind power (Wang et al., 2017), and many other forecasting problems (Makridakis et al., 2020).

In classification applications, there is less consensus on the use of a confidence-based (and hence intuitive) measure of uncertainty. For image classification, for instance, dozens of different uncertainty measures exist (Tagasovska & Lopez-Paz, 2019). Nevertheless, despite the diversity of methods to quantify uncertainty across prediction categories, making uncertainty inferences has converged to a mainstream strategy: the same machine learning model that predicts a given target *simultaneously* learns the associated uncertainties. These models are often underspecified (D’Amour et al., 2020), giving unreliable predictions under stress tests, and also under distribution shift (Ovadia et al., 2019; Hendrycks & Dietterich, 2019). This unreliability is therefore translated (by design) to how these models assess uncertainty.

A different strategy is then considered in this work: *model* how to predict, as usual, but *measure* the associated predictive uncertainty during validation, using a confidence-based learning method.

This model-agnostic approach to uncertainty estimation is aligned with rising trends in the post-hoc explainability of deep learning models (Barredo Arrieta et al., 2020). That is, a predictive deep learning model is considered as a black box and a second system estimates how uncertain the black box is. Our main motivation in this work is finding a neural network to estimate uncertainty which is (by design) the most transparent one that is possible, therefore not having itself any associated uncertainty due to model specification. This leads us to the extreme case of a non-parametric quantile estimator consisting of a single neuron. A number of synthetic and real-world experiments demonstrate that the proposed quantile estimator has similar accuracy but better efficiency than some state-of-the-art methods.

2 Quantile estimation

Let E be a real random variable with distribution F , so that $\Pr(E \leq \varepsilon) = F(\varepsilon)$. For any $p \in (0, 1)$, a p -th quantile of F is a number r_p satisfying $F(r_{p-}) \leq p \leq F(r_p)$, where the left limit is $F(r_{p-}) := \lim_{z \uparrow r_p} F(z)$. For all *continuous* distribution functions F , of interest here, this becomes

$$F(r_p) = p. \tag{1}$$

If F is a strictly increasing function, then there is only one number satisfying (1). It defines the quantile function $r_p = F^{-1}(p)$. It is our purpose in this work to introduce an efficient non-parametric method to estimate it, and apply it to typical regression problems with no discrete component of F .

2.1 Proposed estimator.

To be able to use a neural network, and at the same time obtain a non-parametric quantile estimator, a single neuron is considered whose weight w_p coincides with the quantile to be learned. Using an independently drawn sample $\varepsilon = (\varepsilon_1, \varepsilon_2, \dots, \varepsilon_m)$ of E of size m , this neuron activates itself to output the empirical distribution function $F_m(w_p) = \frac{1}{m} \sum_{i=1}^m \mathbb{1}(\varepsilon_i \leq w_p)$, making an error $\mathcal{L}(w_p) = [F_m(w_p) - p]^2$ in reaching its target p . After properly initializing w_p , this neuron is trained with gradient descent after smoothing the indicator function $\mathbb{1}(\varepsilon_i \leq w_p) \sim \sigma(\beta(w_p - |\varepsilon_i|))$ using a sigmoid $\sigma(x) = (1 + \exp(-x))^{-1}$; this approximation becomes exact as $\beta \rightarrow \infty$.¹

From Borel’s law of large numbers, $F_m(w_p)$ almost surely tends to $F(w_p)$ for infinite sample size. In this limit, our neuron is trained by minimizing $\mathcal{L}(w_p) = [F(w_p) - p]^2$, so its weight w_p converges to the global minimum r_p by (1). Therefore, the proposed quantile estimator is asymptotically consistent. For reasons that become clearer later, it is called a *Prediction Interval Metric* (PIM). Further theoretical details and link to the source code may be found in the supplementary material.

2.2 Comparison to estimation from the order statistics.

Quantile estimation from ranking the order statistics is a pretty standard technique with at most $O(m)$ complexity. It considers the sample $\varepsilon = (\varepsilon_1, \varepsilon_2, \dots, \varepsilon_m)$ and starts by constructing the order statistics $\varepsilon_{(k)}$ as the k -th smallest value in ε , with $k = 1, \dots, m$. If mp is not an integer, then there is only one value of k for which $(k - 1)/m < p < k/m$; this is called the rank. Since $F_m(\varepsilon) = k/m$ for $\varepsilon_{(k)} \leq \varepsilon < \varepsilon_{(k+1)}$, then a unique p -th quantile is estimated as $\varepsilon_{(k)}$. However, if mp is an integer, an interval of p -th quantiles of F_m exists with endpoints $\varepsilon_{(k)}$ and $\varepsilon_{(k+1)}$, the rank becoming a real-valued index. How to select a representative value from such an interval?

One possibility would be to take the midpoint $(\varepsilon_{(k)} + \varepsilon_{(k+1)})/2$. This is equivalent to Laplace’s “Principle of Insufficient Reason” as an attempt to supply a criterion of choice (Janes, 1957), that is, since there is no reason to think otherwise, the events: the best representative value is $\varepsilon_{(k)}$ or the best representative value is $\varepsilon_{(k+1)}$, are equally likely. Hyndman & Fan (1996) compiled a taxonomy of nine interpolation schemes used by a number of statistical packages. They all add to the arbitrariness of selection of a representative value. Since $\Delta F_m(\varepsilon) \sim 1/m$ as $\Delta \varepsilon \sim \varepsilon_{(k+1)} - \varepsilon_{(k)}$, this arbitrariness has a major impact for small sample size, as shown in Fig. 1, where the confidence interval function $I(p) = r_{(1+p)/2} - r_{(1-p)/2}$ of a standard normal random variable is estimated using all interpolation methods provided by the `NUMPY` library. As observed, PIM does not have such a selection bias and can be more accurate for small sample size (see supplementary material for more experiments).

¹Since $\nabla \mathcal{L}(w_p) \sim \beta$, in practice, the value of β can be jointly selected with the learning rate lr . For most of the experiments in this work, $\beta = 10^3$ with $lr = 0.005$ work well.

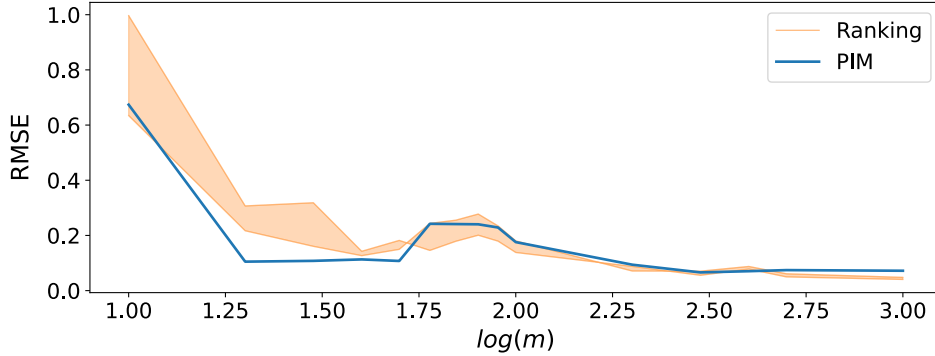


Figure 1: Root Mean Square Error (RMSE) between the estimated and exact confidence interval function $I(p) = r_{(1+p)/2} - r_{(1-p)/2}$ around the median of a standard normal random variable as a function of the log of sample size. The values of p are in the range $[0.05, 0.90]$ in steps of 0.05.

2.3 Conditional quantiles

In regression analysis, one is interested in explaining the variations of a target random variable Y taking values $y \in \mathbb{R}$ in terms of feature random variables X taking values $x \in \mathbb{R}^d$. It is usually assumed, either implicitly or explicitly, that a deterministic map f exists, explaining such variations as $y = f(x) + \varepsilon_{\text{obs}}(x)$, up to some additive noise $\varepsilon_{\text{obs}}(x)$ inherent to the data observation process. Empirically, this map is estimated by choosing a statistical model $\hat{f}(x)$ (e.g. a neural network), which approximates the target as

$$y = \hat{f}(x) + \varepsilon(x). \quad (2)$$

In so doing, the predictive model makes the error $\varepsilon(x) = \varepsilon_{\text{obs}}(x) + \varepsilon_{\text{epis}}(x)$ consisting of the aleatoric part $\varepsilon_{\text{obs}}(x)$ and an epistemic part $\varepsilon_{\text{epis}}(x) = f(x) - \hat{f}(x)$ which entails an uncertainty due to the lack of knowledge of $f(x)$. This could be because we are not sure how to select \hat{f} (model specification) or because the shape of f for unexplored regions of feature space might be significantly different from that inferred from the training set (distributional changes).

The random variable E defined previously is now conditioned on X , which is denoted as $E|X$. It will be understood to take the error values $\varepsilon(x)$ in (2), and is relocated to satisfy $\text{median}(E|X) = 0$. We say that the errors are *homoskedastic* if E is independent of X , otherwise they are *heteroskedastic*. There are then two ways to calculate the aleatoric uncertainty of the target variable Y :

1. Estimating the conditional quantile function $\mu_p(x)$ which assigns pointwise the smallest μ for which $\Pr(Y \leq \mu|x) = p$ and, from this, computing the prediction intervals $[\hat{\mu}_{(1-p)/2}(x), \hat{\mu}_{(1+p)/2}(x)]$ quantifying the uncertainty of the target at confidence level p .
2. Estimating the conditional quantile function $r_p(x)$ of the error variable $E|X$ and computing the corresponding prediction intervals $[\hat{f}(x) - \hat{r}_p(x), \hat{f}(x) + \hat{r}_p(x)]$ quantifying the uncertainty of the target at confidence level p . This assumes that \hat{f} is a good approximator of the median of $Y|X$.

Approaches of type 1 are known as quantile regression. They enlarge the model $\hat{f} \rightarrow (\hat{f}_L, \hat{f}_U)$ to fit the endpoints of the prediction intervals, i.e. $\hat{f}_{L;p}(x) = \hat{\mu}_{(1-p)/2}(x)$ and $\hat{f}_{U;p}(x) = \hat{\mu}_{(1+p)/2}(x)$. Given a training set $\{(x_i, y_i) : i \in \mathcal{I}\}$, we consider two state-of-the-art methods of this kind

- **Simultaneous Quantile Regression (SQR)**: this minimizes the average pinball loss $\frac{1}{|\mathcal{I}|} \sum_{i \in \mathcal{I}} l_p(\varepsilon_i)$ for $\varepsilon_i = y_i - \hat{f}_{L;p}(x_i)$ and for $\varepsilon_i = y_i - \hat{f}_{U;p}(x_i)$ simultaneously in the same model, where $l_p(\varepsilon_i) = p \varepsilon_i \mathbb{1}(\varepsilon_i \geq 0) + (p-1) \varepsilon_i \mathbb{1}(\varepsilon_i < 0)$. This is enough for our purpose, since it has less execution steps than the state-of-the-art SQR of Tagasovska & Lopez-Paz (2019). Yet, it works better than standard quantile regression which estimates each quantile separately.

- **Quality Driven (QD) method** (Pearce et al., 2018): In the training subset indexed by $\mathcal{C} = \{i : \hat{f}_{L;p}(x_i) \leq y_i \leq \hat{f}_{U;p}(x_i)\}$, this minimizes the captured mean prediction interval width (MPIW), which is expressed as $\text{MPIW}_{\text{capt}} = \frac{1}{|\mathcal{C}|} \sum_{i \in \mathcal{C}} [\hat{f}_{U;p}(x_i) - \hat{f}_{L;p}(x_i)]$, subject to the prediction interval coverage proportion (PICP) satisfying $\text{PICP} := |\mathcal{C}|/|\mathcal{I}| \geq p$. The rationale is that prediction intervals of good quality (Khosravi et al., 2011b) have $\text{MPIW}_{\text{capt}}$ as small as possible and enough coverage.

For approaches of type 2, the training set has to be split into two disjoint subsets: a proper training set $\{(x_i, y_i) : i \in \mathcal{I}_1\}$ and a calibration (or validation) set $\{(x_i, y_i) : i \in \mathcal{I}_2\}$. The proper training set is used to fit $\hat{f}(x)$, which is then evaluated on the validation set to compute the errors $\varepsilon_i := \varepsilon(x_i) = y_i - \hat{f}(x_i)$ and their quantiles. This is the setting used in the split conformal prediction literature (Lei et al., 2018), where sample quantiles are estimated by ranking the order statistics. However, in this literature, a single \hat{r}_p is obtained from $\{\varepsilon_i : i \in \mathcal{I}_2\}$. PIM may also be applied within this setting, obtaining $\hat{r}_p(x)$ which could vary with x .

In order to obtain variable $\hat{r}_p(x)$ with PIM, a different neuron u_i has to be used for each position $\{x_i : i \in \mathcal{I}_2\}$. If the data-generating distribution is known (or may be properly approximated), this is used to sample extra targets $\{y_{i;k} : k \in \mathcal{J}\}$ not known to \hat{f} , so PIM estimates the quantiles from the neuron u_i having access to the errors $\varepsilon_{i;k} = y_{i;k} - \hat{f}(x_i)$ for $k \in \mathcal{J}$. A synthetic example of this is shown in Fig. 2. If the data-generating distribution is unknown, but serial correlations are important (i.e. the order of i in \mathcal{I} matters), then PIM may be applied if relative rather than absolute positions in feature space are relevant. This is done by having $|\mathcal{T}|$ different neurons u_j learn quantiles from samples $W_i = [\varepsilon_i, \varepsilon_{i+1}, \dots, \varepsilon_{i+|\mathcal{T}|-1}]$ of the joint error distribution for $i = 1, 2, \dots, |\mathcal{I}_2| - |\mathcal{T}| + 1$, provided there are enough samples in the validation set. By rolling the window W_i , a new sample from the joint distribution is obtained, and the neuron u_j is trained with all the errors observed at the j -th position of all windows. A real-world example of this is shown in Fig. 3. These two examples are described in more detail next.

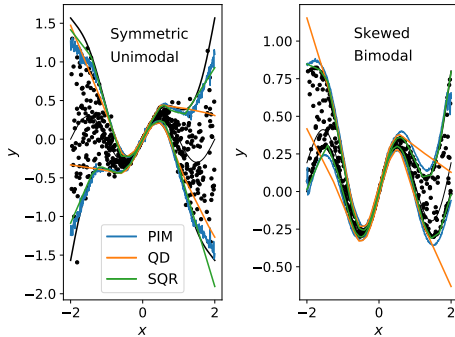


Figure 2: Prediction intervals with 95% confidence estimated by PIM, QD and SQR for synthetic data (black points) normally distributed and with a skewed Beta distribution. The black thick lines are the ideal boundaries, whereas the thin lines are the medians of the distributions.

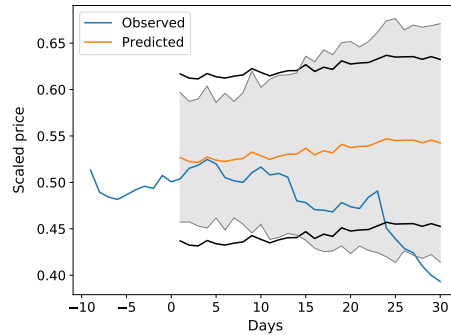


Figure 3: Predicted and observed scaled price of the stock of General Electric for a horizon of $h = 30$ days. The gray area are 95% prediction intervals estimated by PIM; the black lines correspond to bounds based on a baseline assuming normally distributed errors.

Synthetic experiment. The aim here is to compare the accuracy and computational efficiency of PIM against QD and SQR. For this, consider a one-dimensional data-generating process described by $y(x) = 0.3 \sin(x) + \varepsilon_{\text{obs}}(x)$ where $X \sim U(-2, 2)$. For the error associated with observation, two cases are considered — both having scale $\sigma(x) = 0.2x^2$. The first is Gaussian error $E_{\text{obs}}|X \sim N(0, \sigma^2(x))$, exemplifying a symmetric, unimodal distribution. The second is $E_{\text{obs}}|X \sim \text{Beta}(a, b, \text{loc} = 0, \text{scale} = \sigma(x))$, exemplifying a skewed, bimodal distribution when $a < 1$ and $b < 1$. For concreteness, take $a = 0.2$ and $b = 0.3$.

The conditional quantiles of the target may be expressed as $\mu_p(x) = 0.3 \sin(x) + \sigma(x)\mu_p$, where μ_p is the quantile function of the standardized error variable (computed by most statistical libraries for

known distributions). From this, prediction intervals $[\mu_{(1-p)/2}(x), \mu_{(1+p)/2}(x)]$ may be calculated for the two cases of interest — bounded by the black thick lines in Fig. 2 for $p = 0.95$. For visual aid of the symmetry/skewness of the distributions, the median $\mu_{0.5}(x)$ is also shown as thin lines.

In a single trial of the experiment, a neural network \hat{f} with 100 hidden units and output layer with *one* unit is trained by sampling 500 pairs $P = \{(x_i, y_i) : i \in \mathcal{I}\}$, shown as black points in Fig. 2. Since this experiment is synthetic, there is no need to split the training set. Instead, \hat{f} is evaluated on a grid $G = \{x_j : j \in \mathcal{T}\}$ disjoint to P , partitioning $[-2, 2]$ in 500 intervals of equal length. PIM is trained² on G by sampling $|\mathcal{J}| = 1000$ values of $y(x_j)$ for each x_j in G , each neuron u_j learning quantiles from $\{\varepsilon_{j,k} = y_k(x_j) - \hat{f}(x_j) : k \in \mathcal{J}\}$. QD and SQR both train a neural network with 100 hidden units and output layer with *two* units (\hat{f}_L, \hat{f}_U) . The model has the same hyperparameters as \hat{f} . However, for a fair comparison, the training set of (\hat{f}_L, \hat{f}_U) is P augmented with $|\mathcal{J}|$ more pairs disjoint to G . The results for a trial are shown in Fig. 2.

Table 1: Evaluating accuracy and efficiency of quantile estimation by three different methods. The results show median \pm absolute median deviation over the trials. The notation 0.036 ± 0.001 is simplified to $0.036(1)$.

METHOD	# PARAMETERS	TIME	RMSE
SQR	402	0.080 (9)	0.09 (3)
QD	402	0.042 (8)	0.55 (1)
\hat{f} + PIM	301	0.036 (1)	0.218 (3)

The experiment is repeated for 10 trials. For each of them, the time taken to train + evaluate the models (\hat{f}_L, \hat{f}_U) — and to train and evaluate \hat{f} + train PIM — is measured and normalized by the total duration of the 10 experiments. This together with the RMSE between estimations and ideal values is shown in Table 1 for the case of normally distributed noise. As observed, the quantile estimation using PIM has less time and parameter complexity and thus more computationally efficient. In terms of accuracy, \hat{f} + PIM ranks in between SQR and QD despite the fact that \hat{f} is trained with less data and has less parameters than (\hat{f}_L, \hat{f}_U) .

Real-world experiment The aim here is to demonstrate that PIM may be used in realistic contexts where varying prediction intervals are needed, specially when the uncertainty of interest is related to relative rather than absolute positions in feature space. As an illustration, the uncertainty in the prediction of the stock price of General Electric is considered. A LSTM model \hat{f} learns to map features of the last $T = 10$ observations to the next $h = |\mathcal{T}| = 30$ target close prices. This is done in a training set with the first 9840 samples of daily data from 1962 to 2001. The trained model \hat{f} is evaluated on a validation set consisting of the next 4218 samples, where PIM learns prediction intervals corresponding to h consecutive predictions, using neurons u_j for $j \in \mathcal{T}$. These are placed around the predictions on the held-out *test* set shown in Figure 3. These are compared with a popular baseline (Hyndman & Athanasopoulos, 2018), consisting of bounds $\pm z_p \hat{\sigma}_h$ derived by assuming that the errors are normally distributed, with z_p being the z-score. If the forecasts of all h future prices in the test set are assumed to coincide with the average of the past T observations (which is roughly the case in Fig. 3), then it can be shown that $\hat{\sigma}_h = \hat{\sigma} \sqrt{1 + 1/T}$, where $\hat{\sigma}$ is the standard deviation of the h error samples in the test set.

Apart from PIM having better coverage than the baseline and having narrower prediction interval widths at the beginning of the test sequence (hence better quality), this example shows how PIM captures the epistemic uncertainty resulting from \hat{f} knowing better that predictions for tomorrow should be close (by continuity of f) to observations today, giving rise to the cone-shaped uncertainty region. This information is cheap to obtain: while the inference time of the LSTM is about 3.9 sec, PIM only takes about 0.4 sec to obtain the prediction intervals from the validation set.

²For skewed distributions, two neurons independently learn \hat{r}_p^L and \hat{r}_p^U from $\varepsilon \leq 0$ and $\varepsilon > 0$ respectively; the prediction intervals estimated as $[\hat{f} - \hat{r}_p^L, \hat{f} + \hat{r}_p^U]$.

3 Would you use a single neuron to estimate uncertainty?

It has been shown that training a model \hat{f} that learns the mean — hopefully equal or close to the median — of the target distribution and using PIM to estimate its quantiles is more efficient and has similar accuracy than having a bigger model (\hat{f}_L, \hat{f}_U) learning the boundaries of the prediction intervals directly. Also, the quantile estimation for small sample size can be more accurate using PIM than ranking the order statistics. With all these benefits, would you use it in your applications?

The answer to this depends on the dataset. Since the training set has to be split into a proper training set $\{(x_i, y_i) : i \in \mathcal{I}_1\}$ to fit \hat{f} and a validation set $\{(x_i, y_i) : i \in \mathcal{I}_2\}$ to train PIM, the resulting size $|\mathcal{I}_2|$ of the validation set might not be enough for PIM to get accurate results. Also, the amount of heteroskedasticity in the dataset may invalidate using a single neuron learning \hat{r}_p . The effect of these two factors is investigated next for real-world datasets, having the results from QD as a baseline. That is, we follow the experimental protocol established by Hernández-Lobato & Adams (2015) for the popular UCI regression benchmark. This assigns 90% of the data (from 10 different datasets) for training uncertainty estimation models and 10% for testing them, in an ensemble of mostly 20 random shuffles of the train-test partition.

To apply PIM, the 80% of the resampled training set of each dataset is used to train the nominal neural network \hat{f} , which is evaluated on the remaining 20%, where PIM is trained from the corresponding prediction errors. The best between $[\hat{f} - \hat{r}_p, \hat{f} + \hat{r}_p]$ and $[\hat{f} - \hat{r}_p^L, \hat{f} + \hat{r}_p^U]$, in addressing coverage and quality in the *test* sets, is chosen. Therefore, the test MPIW of the QD method is compared to either $2\hat{r}_p$ or $\hat{r}_p^L + \hat{r}_p^U$, depending on which is smaller, and which PICP (which is nothing but the F_m of section 2.1) is closer to the nominal $p = 0.95$. As in the synthetic experiments of the previous section, note that the QD model, besides having more outputs \hat{f}_L and \hat{f}_U (hence more weights), is trained on more data than \hat{f} .

A measure of heteroskedasticity of the datasets is needed in order to better understand the resulting estimations. For this, a White test (White, 1980) is done in every fold used to train PIM. This looks for linear dependency of the variance $\mathbb{E}(\xi^2)$ of residuals ξ (from a linear regression of y on x) on all features in x and their interactions. The proportion of significant tests in the ensemble, according to the p-value of the F-statistic, is denoted by P_{SIG} and reported as a percentage. This gives the percentage of times that the null hypothesis of homoskedastic residuals is rejected; giving a sense of residual variability among the validation folds of the ensemble but not how “strong” that variability is within a fold.

To quantify the degree of variability of the residuals ξ_i used for the White tests, the *normalized* power spectral entropy (PSE) of such residuals is proposed

$$\text{PSE} = -\frac{1}{\log |\mathcal{I}_2|} \sum_{i \in \mathcal{I}_2} p_i \log p_i, \quad (3)$$

where $p_i = |\xi_i|^2 / \sum_i |\xi_i|^2$ normalizes the square amplitude of the i -th spectral component of ξ (found by a fast Fourier transform). The intuition is that *patterns* in ξ have a low entropy $\text{PSE} \rightarrow 0$ whereas homoskedastic-like residuals (e.g. white noise) have high entropy $\text{PSE} \rightarrow 1$.

The results of the comparison with QD are shown in Table 2, where -ENS is appended to the acronyms of the methods to mean that the results are averages over the ensemble. The first observation is that, despite all datasets being heteroskedastic, the uncertainty estimations made by PIM in the validation sets generalize well into the test sets (better or similar to QD in the shaded cases).

The cases where PIM fails to converge to the desired PICP are those with significant variability among the validation folds (low P_{SIG}) or appreciable presence of patterns in the errors (low PSE), as expected. Data size is also important since *Kin8nm* is comparable to *Concrete* in terms of P_{SIG} and PSE, but the former is more than 8 times bigger than the latter. This data-size dependence is evident from the table, where PIM has good performance mostly for the lower half datasets. For the biggest dataset, PIM does not excel presumably due to better calibrated predictions of QD’s (\hat{f}_L, \hat{f}_U) over the \hat{f} feeding PIM — expected from the flexibility of the former in terms of more network weights and more data to train them.

The second observation is that, in the successful cases, the test PICP achieved by PIM coincides with the intended confidence level $p = 0.95$. As seen, this is not necessarily the case for QD, since it

Table 2: *Test* quality metrics for prediction intervals in relevant datasets: mean \pm std dev over the ensemble. Best results in bold, compared according to the criteria and results in Pearce et al. (2018), that is: if $\text{PICP} \geq 0.95$ for QD and PIM, both were best for PICP, and best MPIW is given to the smallest MPIW. If $\text{PICP} \geq 0.95$ for neither or for only one, largest PICP was best, and MPIW assessed if the one with larger PICP also has smallest MPIW.

DATASET	SIZE	P_{SIG}	PSE	PICP		MPIW	
				QD-ENS	PIM-ENS	QD-ENS	PIM-ENS
YACHT	308	65	0.80 (6)	0.96 (1)	0.90 (6)	0.17 (0)	0.26 (7)
BOSTON	506	70	0.87 (6)	0.92 (1)	0.84 (8)	1.16 (2)	0.7 (1)
ENERGY	768	100	0.80 (2)	0.97 (1)	0.95 (2)	0.47 (1)	0.21 (4)
CONCRETE	1,030	100	0.74 (2)	0.94 (1)	0.90 (4)	1.09 (1)	1.04 (9)
RED WINE	1,599	75	0.78 (2)	0.92 (1)	0.82 (9)	2.33 (2)	1.9 (3)
KIN8NM	8,192	100	0.72 (1)	0.96 (0)	0.95 (1)	1.25 (1)	1.17 (6)
POWER PLANT	9,568	90	0.84 (5)	0.95 (0)	0.95 (1)	0.86 (0)	0.87 (2)
NAVAL	11,934	100	0.88 (1)	0.98 (0)	0.95 (1)	0.28 (1)	0.23 (9)
PROTEIN	45,730	100	0.66 (0)	0.95 (0)	0.94 (0)	2.27 (1)	2.65 (1)
SONG YEAR	515,345	100	0.86 (·)	0.96 (·)	0.95 (·)	2.48 (·)	3.12 (·)

targets $\text{PICP} \geq p$. However, for a *continuous* target variable Y — as in many regression problems of practical interest — $\text{PICP} = p$ must be (asymptotically) satisfied at the p -quantile. Restricting $\text{PICP} \geq p$ in these cases may lead to the same quantile estimation describing different confidence levels; the quantile-crossing phenomenon (Takeuchi et al., 2006) that should be avoided.

The results above show that using PIM with a single neuron may give accurate estimation of high-quality prediction intervals even for heteroskedastic datasets with *weak* serial correlations (i.e. patterns) of the prediction error samples. Therefore, in the exploratory data analysis of a given application, heteroskedasticity tests in the dataset may reveal whether or not to leverage from the efficiency of using a single neuron for uncertainty estimation.

4 Related work

The split conformal prediction literature (Lei et al., 2018) uses a setting similar to PIM, estimating quantiles by ranking the order statistics of prediction errors from a given \hat{f} . They give finite sample coverage guarantees by assuming *exchangeability* of the training samples, which may not apply, for instance, for non-stationary stochastic processes typically found in real-world time series. Recently, Romano et al. (2019) have extended this framework to produce varying $\hat{r}_p(x)$ by combining the split conformal prediction formalism with quantile regression from (\hat{f}_L, \hat{f}_U) . As shown in this work, PIM has the advantage of being more flexible to high-quality quantile estimation from small sample sizes compared to ranking the order statistics. This may be important in those cases for which the size of the validation set is a small fraction of the training set.

Recent research on uncertainty estimation focuses on studying the different sources of uncertainty. Prediction intervals capture the aleatoric uncertainty associated to the noisy data observation process (Pearce et al., 2018; Tagasovska & Lopez-Paz, 2019; Salem et al., 2020). Epistemic uncertainty involves model specification and data distributional changes; the latter maintaining recent interest (Malinin & Gales, 2018; Hafner et al., 2019; Tagasovska & Lopez-Paz, 2019; Li & Hoiem, 2020; Zhe Liu et al., 2020; Charpentier et al., 2020; Postels et al., 2020); the former being less studied. Examples in deep learning of uncertainty due to model specification include network-depth uncertainty (Antorán et al., 2020) and uncertainty over the number of nodes in model selection (Ghosh et al., 2019).

The incompleteness in problem formalization behind machine learning models — intimately connected to model specification — leads to a need for their interpretability (Doshi-Velez & Kim, 2017). This need became more urgent in 2016, when the European Parliament published the General Data Protection Regulation, demanding (among other clauses) that, by May 2018, all algorithms have to provide “meaningful explanations of the logic involved” when used for decision making significantly affecting individuals (right of people to an explanation). Consequently, techniques to explain AI models started to permeate the literature. Ribeiro et al. (2016) made a case for model-agnostic

interpretability of machine learning; while Rudin (2019) argued in favor of designing predictive models that are themselves interpretable. Different reviews arose (Gilpin et al., 2018; Guidotti et al., 2018) to clarify concepts and classify the increasing body of related research.

The current understanding (Barredo Arrieta et al., 2020) is that a model is interpretable if, by itself, is understandable (e.g. linear/logistic regression, decision trees, K -nearest neighbors, rule-based learners, Bayesian models). If not, it needs post-hoc explainability (e.g. tree ensembles; SVM; multi-layer, convolutional and recurrent neural networks). Post-hoc explainability is done by feature relevance analysis or visualization techniques, but most often by a second *simplified*, and hence interpretable, model which mimics its antecedent. Our approach to uncertainty estimation goes along lines similar to the latter: a predictive model \hat{f} is considered as a black box and a second system (at least a single, completely transparent, neuron) estimates how uncertain the black box is.

Although using a model to learn from a black box has been explored in a context related to uncertainty, e.g. calibration of neural networks using Platt scaling (Kuleshov et al., 2018), it was not until recently that such a method is directly used to upgrade any black-box predictive API with an uncertainty score (Brando et al., 2020). However, their wrapper is based on deep neural networks and hence is not interpretable. PIM *is not* a parametric model, but uses globally interpretable neural networks.

5 Conclusion

In this work, a non-parametric method to estimate predictive uncertainty of a pre-trained model is introduced. The method is competitive with state-of-the-art solutions in quality, with the additional benefit of giving uncertainty estimates more efficiently (i.e. no need to add extra layers or outputs to a predictive model). Although the method does not *predict* the uncertainty of new data samples based on their feature values — perhaps making it less attractive, as it deviates from the established machine learning paradigm — it does give a sense of a safer uncertainty estimation, just because it does not inherit the learning biases of the predictive models. This makes it suitable for rather *explaining* how uncertain a given model (treated as a black-box) is, and hence serving as a reliable guide to decision-making. Extensions of the method to estimate uncertainty in the classification setting is given in the supplementary material.

References

- Amodei, D., Olah, C., Steinhardt, J., Christiano, P., Schulman, J., and Mané, D. Concrete Problems in AI Safety. *arXiv e-prints*, art. arXiv:1606.06565, Jun 2016.
- Antorán, J., Urquhart Allingham, J., and Hernández-Lobato, J. M. Depth uncertainty in neural networks. In *34th Conference on Neural Information Processing Systems*, 2020.
- Barredo Arrieta, A. et al. Explainable artificial intelligence (xai): Concepts, taxonomies, opportunities and challenges toward responsible ai. *Information Fusion*, 58:82–115, 2020.
- Brando, A., Torres, D., Rodríguez-Serrano, J. A., and Vitrià, J. Building uncertainty models on top of black-box predictive apis. *IEEE Access*, 8:121344–121356, 2020.
- Charpentier, B., Zügner, D., and Günnemann, S. Posterior Network: Uncertainty Estimation without OOD Samples via Density-Based Pseudo-Counts. In *34th Conference on Neural Information Processing Systems*, 2020.
- Chudý M., Karmakar S., and Wu W. B. Long-term prediction intervals of economic time series. *Empirical Economics*, 58(1):191–222, 2020.
- Cosmides, L. and Tooby, J. Are humans good intuitive statisticians after all? rethinking some conclusions from the literature on judgement under uncertainty. *Cognition*, 58(1):1–73, 1996.
- D’Amour, A. et al. Underspecification Presents Challenges for Credibility in Modern Machine Learning. *arXiv e-prints*, art. arXiv:2011.03395, November 2020.
- Doshi-Velez, F. and Kim, B. Towards A Rigorous Science of Interpretable Machine Learning. *arXiv e-prints*, pp. arXiv:1702.08608, 2017.

- Galván, I. M. et al. Multi-objective evolutionary optimization of prediction intervals for solar energy forecasting with neural networks. *Information Sciences*, 418-419:363–382, 2017.
- Ghosh, S., Yao, J., and Doshi-Velez, F. Model selection in bayesian neural networks via horseshoe priors. *Journal of Machine Learning Research*, 20(182):1–46, 2019.
- Gilpin, L. H. et al. Explaining explanations: An overview of interpretability of machine learning. In *IEEE 5th International Conference on Data Science and Advanced Analytics (DSAA)*, pp. 80–89, 2018.
- Guidotti, R. et al. A survey of methods for explaining black box models. *ACM Computing Surveys*, 51(5), 2018.
- Guo, C., Pleiss, G., Sun, Y., and Weinberger, K. Q. On Calibration of Modern Neural Networks. *arXiv e-prints*, art. arXiv:1706.04599, Jun 2017.
- Hafner, D. et al. Reliable uncertainty estimates in deep neural networks using noise contrastive priors. In *Uncertainty in Artificial Intelligence (UAI)*, 2019.
- Hendrycks, D. and Dietterich, T. Benchmarking neural network robustness to common corruptions and perturbations. In *Proceedings of the International Conference on Learning Representations*, 2019.
- Hernández-Lobato, J. M. and Adams, R. P. Probabilistic backpropagation for scalable learning of bayesian neural networks. In *Proceedings of the 32nd International Conference on Machine Learning*, 2015.
- Huang, S.-F. and Hsu, H.-L. Prediction intervals for time series and their applications to portfolio selection. *REVSTAT – Statistical Journal*, 18(1):131–151, 2020.
- Hyndman, R. and Athanasopoulos, G. *Forecasting: principles and practice*. OTexts, 2018. ISBN 9780987507112.
- Hyndman, R. J. and Fan, Y. Sample quantiles in statistical packages. *American Statistician*, 50:361, 1996.
- IntHout, J. et al. Plea for routinely presenting prediction intervals in meta-analysis. *BMJ Open*, 6(7), 2016.
- Janes, E. T. Information theory and statistical mechanics. *Physical Review*, 106:620–630, 1957.
- Josang, A., Cho, J., and Chen, F. Uncertainty characteristics of subjective opinions. In *21st International Conference on Information Fusion*, pp. 1998–2005, 2018.
- Juanchich, M. and Miroslav, S. Do people really prefer verbal probabilities? *Psychological Research*, 84(8):2325–2338, 2020.
- Khosravi, A. et al. Comprehensive review of neural network-based prediction intervals and new advances. *IEEE transactions on neural networks*, 22:1341–56, 2011a.
- Khosravi, A. et al. Lower upper bound estimation method for construction of neural network-based prediction intervals. *IEEE Transactions on Neural Networks*, 22:337–346, 2011b.
- Krishnan, R. and Tickoo, O. Improving model calibration with accuracy versus uncertainty optimization. In *Proceedings of the 34th Conference on Neural Information Processing Systems*, 2020.
- Kuleshov, V., Fenner, N., and Ermon, S. Accurate uncertainties for deep learning using calibrated regression. In *Proceedings of the 35th International Conference on Machine Learning*, 2018.
- Kumar, A., Liang, P. S., and Ma, T. Verified uncertainty calibration. In *Advances in Neural Information Processing Systems*, 2019.
- Küppers, F. et al. Multivariate confidence calibration for object detection. In *The IEEE/CVF Conference on Computer Vision and Pattern Recognition (CVPR) Workshops*, June 2020.

- Lei, J., G'Sell, M., Rinaldo, A., Tibshirani, R. J., and Wasserman, L. Distribution-free predictive inference for regression. *Journal of the American Statistical Association*, 113(523):1094–1111, 2018.
- Li, Z. and Hoiem, D. Improving confidence estimates for unfamiliar examples. In *Proceedings of the IEEE/CVF Conference on Computer Vision and Pattern Recognition (CVPR)*, 2020.
- Lin'kov, Y. N. *Lectures in Mathematical Statistics: Parts 1 and 2*. American Mathematical Society, 2005. ISBN 978-0821837320.
- Makridakis, S., Spiliotis, E., and Assimakopoulos, V. The m4 competition: 100,000 time series and 61 forecasting methods. *International Journal of Forecasting*, 36(1):54–74, 2020.
- Malinin, A. and Gales, M. Predictive uncertainty estimation via prior networks. In *Proceedings of the 32nd Conference on Neural Information Processing Systems*, 2018.
- Ovadia, Y. et al. Can you trust your model's uncertainty? evaluating predictive uncertainty under dataset shift. In *Advances in Neural Information Processing Systems 32*, pp. 13991–14002. 2019.
- Pearce, T. et al. High-quality prediction intervals for deep learning: A distribution-free, ensembled approach. In *Proceedings of the 35th International Conference on Machine Learning*, 2018.
- Petropoulos, F., Hyndman, R. B., and Bergmeir, C. Exploring the sources of uncertainty: Why does bagging for time series forecasting work? *European Journal of Operational Research*, 268: 545–554, 2018.
- Postels, J. et al. Quantifying Aleatoric and Epistemic Uncertainty Using Density Estimation in Latent Space. *arXiv e-prints*, art. arXiv:2012.03082, December 2020.
- Quan, H., Dipti, S., and Khosravi, A. Uncertainty handling using neural network-based prediction intervals for electrical load forecasting. *Energy*, 73:916–925, 2014.
- Ribeiro, M., Singh, S., and Guestrin, C. Model-Agnostic Interpretability of Machine Learning. In *ICML Workshop on Human Interpretability in Machine Learning*, 2016.
- Romano, Y., Patterson, E., and Candes, E. Conformalized quantile regression. In *Advances in Neural Information Processing Systems*, volume 32, 2019.
- Rudin, C. Stop explaining black box machine learning models for high stakes decisions and use interpretable models instead. *Nature Machine Intelligence*, 1(5):206–215, 2019.
- Salem, T. S., Langseth, H., and Ramampiaro, H. Prediction intervals: Split normal mixture from quality-driven deep ensembles. In *Proceedings of the 36th Conference on Uncertainty in Artificial Intelligence*, 2020.
- Sensoy, M., Kaplan, L., and Kandemir, M. Evidential deep learning to quantify classification uncertainty. In *Advances in Neural Information Processing Systems*, pp. 3179–3189, 2018.
- Shi, W. et al. Multifaceted uncertainty estimation for label-efficient deep learning. In *Proceedings of the 34th Conference on Neural Information Processing Systems*, 2020.
- Sun, X., Wang, Z., and Hu, J. Prediction Interval Construction for Byproduct Gas Flow Forecasting Using Optimized Twin Extreme Learning Machine. *Mathematical Problems in Engineering*, 2017: 5120704, 2017.
- Tagasovska, N. and Lopez-Paz, D. Single-model uncertainties for deep learning. In *Advances in Neural Information Processing Systems 32*, pp. 6414–6425. Curran Associates, Inc., 2019.
- Takeuchi, I. et al. Nonparametric quantile estimation. *Journal of Machine Learning Research*, 7: 1231, 2006.
- Varshney, K. R. and Alemzadeh, H. On the Safety of Machine Learning: Cyber-Physical Systems, Decision Sciences, and Data Products. *arXiv e-prints*, art. arXiv:1610.01256, October 2016.

- Wang, J. et al. Wind power interval prediction based on improved pso and bp neural network. *Journal of Electrical Engineering and Technology*, 12(3):989–995, 2017.
- White, H. A heteroskedasticity-consistent covariance matrix estimator and a direct test for heteroskedasticity. *Econometrica*, 48:817–838, 1980.
- Zhang, J. Estimating confidence intervals on accuracy in classification in machine learning. Master’s thesis, University of Alaska, 2019.
- Zhe Liu, J. et al. Simple and principled uncertainty estimation with deterministic deep learning via distance awareness. In *Proceedings of the 34th Conference on Neural Information Processing Systems*, 2020.

Supplementary information

A theoretical ground is given here to key aspects of the paper together with extra details about the numerical experiments³. Moreover, PIM is applied to binary classification in order to give more support to the claim that it can be more accurate than ranking the order statistics for small sample size. This is done, on real-world datasets, by comparing confidence intervals for the accuracy of classification, as estimated by PIM, with the corresponding estimations using the Bootstrap method.

The material in the following is organized as follows: section S.1 summarizes the main theoretical assumptions behind PIM, making it an asymptotically consistent estimator. A heuristic for identification of finite-sample convergence is discussed in section S.1.1. Details about the regression experiments using the UCI datasets are given in section S.2. Finally, section S.3 applies PIM in the classification context. It starts in section S.3.1 with the problem formulation and proceeds with the experimental results comparing PIM with the Bootstrap method. A proof of the main theoretical result of the section is given in S.3.2, and details of the experiments are found in section S.3.4.

S.1 PIM as a consistent estimator

The main result is summarized in Theorem 1 below. In order to prove it, we go in steps by first showing that for the distribution functions of interest, the p -th quantile is unique, given the confidence level p . This uniqueness guarantees that the loss function of PIM has asymptotically only one minimum and then gradient descent will converge to it, given small enough learning rates. The uniqueness is proved in the following lemma:

Lemma 1. *Let $F(\varepsilon) = \Pr(E \leq \varepsilon)$ be a strictly increasing and continuous distribution function and $p \in (0, 1)$. Then, the p -quantile r_p is unique.*

Proof. A p -quantile of F is a number r_p satisfying $F(r_p) \leq p$ and $F(r_p + \epsilon) \geq p$, for $\epsilon \rightarrow 0^+$ Lin'kov (2005). Since F is continuous, Bolzano's theorem states that there is at least one point in the interval $[r_p, r_p + \epsilon]$ where $F(r_p) - p = 0$. That there is only *one* such point clearly follows from F being strictly increasing. Therefore, as $\epsilon \rightarrow 0^+$, r_p becomes the unique value where $F(r_p) = p$. \square

Lemma 2. *Let $\{\varepsilon_i\}$, with $i = 1, 2, \dots, m$, be a sequence of independent draws of the random variable E , according to the distribution $F(\varepsilon) = \Pr(E \leq \varepsilon)$. With $\mathbb{1}$ being the indicator function, define $F_m(r_p) = \frac{1}{m} \sum_{i=1}^m \mathbb{1}(\varepsilon_i \leq r_p)$. Then, for all r_p and with probability one, $F_m(r_p)$ converges to $F(r_p)$ in the limit $m \rightarrow \infty$.*

Proof. This is Borel's law of large numbers. \square

Theorem 1. *Let $F(\varepsilon) = \Pr(E \leq \varepsilon) = \int_{-\infty}^{\varepsilon} \rho(x)dx$ be a strictly increasing and continuous error distribution function associated to the random variable E , with ρ being the corresponding probability density function. If m samples are independently drawn from it, then PIM (with $\beta \rightarrow \infty$) evaluated on these samples, converges to the unique value r_p for which $F(r_p) = p$, when $m \rightarrow \infty$.*

Proof. In the limit $\beta \rightarrow \infty$, the $F_m(r_p)$ in PIM coincides with the $F_m(r_p)$ in Lemma 2. Using this Lemma, the loss function in PIM is asymptotically $\mathcal{L}_p(\varepsilon) = (F(\varepsilon) - p)^2$. Its gradient is $\nabla_{\varepsilon} \mathcal{L}_p(\varepsilon) = 2[F(\varepsilon) - p] \rho(\varepsilon)$. Since ε is in the support of E , $\rho(\varepsilon) \neq 0$, then gradient descent, with a small enough learning rate, leads PIM to converge to the value of ε for which $F(\varepsilon) - p = 0$. By Lemma 1, there is only one such value, being the p -quantile r_p . \square

S.1.1 Convergence for finite validation sets

It is observed in the numerical experiments that the loss in PIM smoothly decreases and saturates about a small value. By using early stopping during optimization, the optimal value \hat{r}_p is taken as the point where this saturation takes place. It is argued in this section why such heuristic approach makes sense. For this, it is convenient to think of the current value w_p of the weight of the single neuron as following a trajectory parameterized by the epochs.

³The source code can be found at <https://github.com/sola-ed/pim-uncertainty>

In practice, w_p is updated when the optimizer processes a batch and, at the end of a training epoch, all batches have been processed. The training epochs can then be thought of as values achieved by a continuous variable t , which changes as w_p goes from its initial value, along a *smooth* trajectory $w_p(t)$, to the optimal value \hat{r}_p . Without loss of generality, it is supposed that these trajectories have no turning points, i.e. they monotonically increase or decrease the initial value $w_p(0)$ towards \hat{r}_p . Furthermore, the rate at which this happens is bounded:

$$|\nabla_t w_p(t)| \leq c_p, \quad \text{with } 0 < c_p < \infty. \quad (4)$$

From the proof of Theorem 1 for infinite sample size, $\nabla_\varepsilon \mathcal{L}_p(\varepsilon) = 2[F(\varepsilon) - p] \rho(\varepsilon)$, so from (4),

$$|\nabla_t \mathcal{L}_p(t)| \leq 2c_p |F(w_p(t)) - p| \rho(w_p(t)). \quad (5)$$

A hypothetical algorithm, running with infinite validation set, will start at $t = 0$, from $w_p(0)$, with successive updates generated (assuming a plain SGD optimizer) as

$$w_p(t + dt) = w_p(t) - \eta \nabla_t \mathcal{L}_p(t), \quad (6)$$

where η is the learning rate and $dt = B/m$, with B and m being the batch and validation set sizes, respectively. The sizes B and m can be selected so that dt is fixed, and arbitrarily small, when $B \rightarrow \infty$ and $m \rightarrow \infty$.

The convergence of PIM to the optimal value \hat{r}_p can be considered, in practical terms, as related to the saturation of the loss function $\mathcal{L}_p(t)$. Given a small enough tolerance σ_p , the algorithm is said to converge to \hat{r}_p at epoch t_* if $|\nabla_z \mathcal{L}_p(t_*)| \leq \sigma_p$, at which point the loss has saturated. If PIM is stopped at t_* , the error committed in estimating the p -quantile of F is, up to first order in σ_p ,

$$|r_p - \hat{r}_p| = \frac{\sigma_p}{2c_p [\rho(r_p)]^2}, \quad (7)$$

which is obtained by evaluating (5) at t_* , writing $\hat{r}_p = w_p(t_*)$, and expanding F and ρ around r_p , giving $|\nabla_t \mathcal{L}_p(t_*)| \leq \sigma_p$.

Finite validation sets. In this case, the trajectories are not generated by (6) anymore. Here, dt is not arbitrarily small, i.e. $\min\{dt\} = 1/m$, which happens when a batch contains only one data sample.⁴ The trajectories are still considered smooth and with bounded speed, but now the values of w_p updated by PIM are more sparse. These trajectories are generated by the loss $\mathcal{L}_p^m(t) = [F_m(t) - p]^2$, i.e.

$$w_p(t + dt) = w_p(t) - \eta \nabla_t \mathcal{L}_p^m(t).$$

Assuming the same constants c_p serve as upper bounds to all the possible speeds,

$$|\nabla_t \mathcal{L}_p^m(t)| \leq 2c_p |F_m(w_p(t)) - p| |F'_m(w_p(t))|. \quad (8)$$

Saturation of the loss is understood as making (8) as small as possible. Clearly, since the gradient $F'_m(w_p(x))$ is bounded and does not vanish, this saturation happens at the epoch t_* of closest approach between $F_m(w_p(t))$ and p , that is,

$$t_* = \arg \min_{t \in [0, \infty)} |F_m(w_p(t)) - p|.$$

Again, denoting $\hat{r}_p = w_p(t_*)$, and using the triangle inequality,

$$|F_m(\hat{r}_p) - p| \leq |F_m(\hat{r}_p) - F(\hat{r}_p)| + |F(\hat{r}_p) - p|,$$

the right-hand side approaching zero, by Lemma 2 and Theorem 1, as more data is considered in the validation set. This explains why early stopping was used throughout the numerical experiments, by automatically detecting t_* and retrieving the corresponding \hat{r}_p .

⁴In practice, the batch size was taken to be equal to the sample size though in order to exploit the asymptotic properties behind PIM.

S.2 Details of models on UCI regression datasets

The baseline model has one relu-activated hidden layer with 50 units, except for *Protein* and *Song Year*, having 100 units. The ensembles are 20 repetitions of the experiments, except for *Protein* and *Song Year*, for which only 5 and 1 repetitions are considered, respectively. Hyperparameter optimization is done using the Hyperband tuner in Keras. For this, two protocols were tried and the best of the two, for each dataset, reported:

1. Optimization of learning rate, decay rate, weight-initialization variance, and dropout rate (using the Adam optimizer).
2. Optimization of weight-initialization variance, weight decay, initial learning rate, and the decay rate of its subsequent exponential decay in a learning rate schedule (using the AdamW optimizer).

In both protocols, the mean square error loss is used. However, in the second protocol, the CWC value (Khosravi et al., 2011a) is added to the metric used in the validation set for model selection in the hyperparameter optimization process. This value is calculated as $CWC = NMPIW(1 + \gamma e^{-\eta(\text{PICP}-p)})$, where NMPIW is the MPIW normalized to the range of the target variable, $\gamma = \mathbb{1}(\text{PICP} < p)$ and η is a constant taken as 0.1. The PICP and MPIW are calculated by PIM.

S.3 PIM for classification

In classification problems, the target Y is a *discrete* random variable, but these can be framed so that the prediction error $E|X$ is still a continuous random variable accessible to PIM. The aim of this section is twofold:

- Give additional demonstration that PIM can be more accurate for small sample sizes than ranking the order statistics, by using real-world datasets for binary classification.
- Demonstrate that using PIM to estimate confidence intervals for the accuracy of a classifier is more efficient than standard computations based on the Bootstrap method.

To better illustrate the problem consider a sample $\{\hat{f}(x_i) \in [0, 1] : i \in \mathcal{I}_2\}$ of predictions from a binary classifier. Denoting by $\llbracket y \rrbracket$ the rounding operation, the accuracy of the classifier is

$$\text{ACC} = \frac{1}{|\mathcal{I}_2|} \sum_{i \in \mathcal{I}_2} \mathbb{1}(\llbracket \hat{f}(x_i) \rrbracket = y_i). \quad (9)$$

How do we estimate a confidence interval for the accuracy? The simplest way is by using the normal approximation to the binomial result:

$$\delta_p(\text{ACC})_{\mathcal{N}} = z_p \sqrt{\hat{\mu}_{\text{ACC}}(1 - \hat{\mu}_{\text{ACC}}) / |\mathcal{I}_2|}, \quad (10)$$

where z_p is the z-score and $\hat{\mu}_{\text{ACC}}$ is an estimation of the mean μ_{ACC} of the distribution of accuracies. Clearly, using ACC in (9) as a substitute for $\hat{\mu}_{\text{ACC}}$ is rough; that is the standard way of getting confidence intervals for accuracy from one sample of predictions.

The standard estimation can be improved by resampling the proper training and validation sets, \mathcal{I}_1 and \mathcal{I}_2 , respectively. That is, by the de Moivre-Laplace central limit theorem, all the so-obtained values of ACC are asymptotically normally distributed around μ_{ACC} , so their mean $\hat{\mu}_{\text{ACC}}$ is an unbiased estimator of μ_{ACC} . When the resampling is done with repetition (a.k.a. the Bootstrap method), in order to allow for enough data, confidence intervals can be estimated by ranking the order statistics of all ACC, instead of using (10).

One of the main observations in this section is that, provided that \hat{f} is well calibrated, PIM can estimate confidence intervals $\delta_p(\text{ACC})$ for the accuracy of a classifier, which are good estimates even when using a single sample of predictions. This is formalized and proved in section S.3.2. Since it would not need to resample the validation set, this makes PIM more efficient than the Bootstrap method. Experiments comparing PIM with the two methods above are described next.

Table S1: Comparison of Bootstrap vs PIM estimation of 95% confidence interval widths for the accuracy of classification algorithms on UCI data sets: median \pm median absolute deviation over the ensemble. Binomial estimates according to (10) are in the last column $2\delta_p(\text{ACC})_{\mathcal{N}}$.

DATASET	SIZE	p_N	$\hat{\mu}_{\text{ACC}}$	Δ_{CALIB}	$2\delta_p(\text{ACC})$		$2\delta_p(\text{ACC})_{\mathcal{N}}$
					BS-ENS	PIM-ENS	
SONAR	208	0.47	0.87	0.00	0.31 \pm 0.07	0.16 \pm 0.07	0.23
HEART DISEASE	303	0.46	0.86	0.00	0.35 \pm 0.05	0.25 \pm 0.09	0.17
IONOSPHERE	351	0.36	0.88	0.00	0.19 \pm 0.04	0.19 \pm 0.05	0.15
MUSK	476	0.43	0.91	0.00	0.21 \pm 0.05	0.14 \pm 0.05	0.11
BREAST CANCER	569	0.34	0.96	0.00	0.07 \pm 0.02	0.07 \pm 0.04	0.06
PIMA DIABETES	768	0.35	0.75	0.00	0.07 \pm 0.01	0.20 \pm 0.10	0.14
SPAMBASE	4,601	0.39	0.94	3.47	0.10 \pm 0.02	0.06 \pm 0.01	0.03
PHONEME	5,404	0.29	0.81	2.07	0.00 \pm 0.00	0.11 \pm 0.01	0.05
MAMMOGRAPHY	11,183	0.02	0.99	0.00	0.00 \pm 0.00	0.08 \pm 0.07	0.01

S.3.1 Benchmarking experiments

For binary classification, the target Y is either 0 (negative class) or 1 (positive class). Predictive models capture this by making predictions $\hat{f}(x) \in [0, 1]$. According to the chosen threshold τ (here $\tau = 1/2$), these are positive predictions if $\hat{f}(x) > \tau$, otherwise they are negative. Furthermore, by comparing with the corresponding ground truth, each prediction may be categorized as true negative, true positive, false negative, or false positive; denoted, respectively, by the index $l \in \{\text{TN}, \text{TP}, \text{FN}, \text{FP}\}$.

Relevant metrics of model performance are derived from the classification rates R_k . For instance, the accuracy can be written as $\text{ACC} = p_N R_{\text{TN}} + p_P R_{\text{TP}}$, where p_N (p_P), are the negative (positive) class proportions in the validation set. Confidence intervals for accuracy are then obtained as

$$\delta_p(\text{ACC}) = p_N \delta_p(R_{\text{TN}}) + p_P \delta_p(R_{\text{TP}}), \quad (11)$$

in terms of confidence intervals for the classification rates $\delta_p(R_l)$. The latter are estimated by PIM after estimating quantiles from the error samples $\varepsilon_l(x) = y_l - \hat{f}(x)$ observed in the validation set, where y_l is the ground truth label if l refers to a *true* prediction, otherwise $y_l = \tau$. For this, four neurons s_l are trained in parallel until the optimal weights \hat{r}_p^l estimate the desired quantiles.

As stated in Theorem 2, the success of PIM depends on being fed by the outputs of a well-calibrated classifier (Guo et al., 2017; Kuleshov et al., 2018; Krishnan & Tickoo, 2020), so that these outputs approximate true probabilities. In these cases, PIM will give high-quality uncertainty estimates for the classification rates and derived quantities, given enough data. For the experiments that follow, a lower bound Δ_{calib} for the calibration error of the uncalibrated models is calculated by the method introduced in Kumar et al. (2019).

To run the experiments, a classification model \hat{f} with one hidden layer (having as many units as data features) and a sigmoid-activated output, is trained on 80% of the data and evaluated on the remaining 20%, for nine UCI datasets. To quantify the spread of the uncertainty estimations, the train-test partition is randomly shuffled multiple times, forming an ensemble of 30 experiments.

For each experiment, the distribution of ACC is sampled $B = 20$ times by training \hat{f} on B transformations of the original training set, obtained by randomly sampling from it with replacement. Confidence intervals from the B accuracies obtained in the validation (=test) sets are then computed by ranking their order statistics. The results from this Bootstrap (BS) method are compared with PIM and the binomial estimate in Table S1. As observed, PIM obtains confidence interval widths which are often narrower than BS (which ranks the order statistics of ACC) and therefore of higher quality, specially for small sample sizes. Yet, these are accurate enough⁵ to overlap with the binomial estimate (except those few cases where \hat{f} is miscalibrated). Benchmarking PIM against BS is important since the latter is a popular method (Zhang, 2019), used for addressing uncertainties in many real-world applications, including time series forecasting (Petropoulos et al., 2018).

⁵The effect of calibration on the spread of uncertainty estimations is investigated in section S.3.4

S.3.2 Theoretical details

The main theoretical result of section S.3, namely Theorem 2, is proved in this section. It will be understood that \hat{Y} is a random variable taking the continuous values $\hat{y} = \hat{f}(x) \in [0, 1]$. Using the classification threshold τ (by default $\tau = 0.5$), \hat{Y} is compared to the ground truth binary variable Y , taking values $y \in \mathcal{B} = \{0, 1\}$, by applying the *rounding* operation, $[\hat{Y}]_\tau = \mathbb{1}(\hat{Y} > \tau)$, which projects the values to the binary set \mathcal{B} .

Definition 1. The index l has been defined as a label for the set $\mathcal{K} = \{\text{TN}, \text{TP}, \text{FN}, \text{FP}\}$. This index can be written as the cartesian product $l = s_l \times v_l = \{(s_l, v_l) : s_l \in \{\text{T}, \text{F}\} \text{ and } v_l \in \{\text{N}, \text{P}\}\}$. A mapping to the binary set \mathcal{B} is introduced by putting a bar above the respective symbols according to:

$$\bar{s}_l = \bar{v}_l \in \mathcal{B} \text{ for } s_l = \text{T}, \text{ and } \bar{s}_l = 1 - \bar{v}_l \in \mathcal{B} \text{ for } s_l = \text{F}.$$

In this way, a value of l can be uniquely mapped to a pair of binary symbols (\bar{s}_l, \bar{v}_l) , taking on values in \mathcal{B} . Just as the rounding operator $[\cdot]_\tau \equiv [\cdot]_v$ projects to the set $\{\text{N}, \text{P}\}$ of possible values of v_l , we define $[\cdot]_s$ as an operator projecting to the set $\{\text{T}, \text{F}\}$ of possible values of s_l . Unless otherwise stated, the subscript τ may be dropped, for simplicity, from the rounding operator $[\cdot]_\tau$.

Definition 2. The symbol $|a|$ is used to count the total number of elements in the set labeled by a ; for instance, the quantity $|v_l| \in \{|\text{N}|, |\text{P}|\}$ takes on values denoting the total number of negatives or positives in the validation set. Using this notation, the classification rates $R_l = L_l/V_l$ can be written as a quotient of random variables L_l and V_l taking on the values, $|l|$ and $|v_l|$, respectively.

Lemma 3. *The classification rates $R_l = L_l/V_l$ are asymptotically normal distributed with mean $\Pr([\hat{Y}] = \bar{s}_l | Y = \bar{v}_l)$ and variance $|v_l|^{-1} \Pr([\hat{Y}] = \bar{s}_l | Y = \bar{v}_l) \Pr([\hat{Y}] = 1 - \bar{s}_l | Y = \bar{v}_l)$ in the limit when $|v_l| \rightarrow \infty$.*

Proof. Since $[\hat{Y}]$ is a binary random variable, L_l is Binomially distributed, so the result immediately follows after applying the de Moivre-Laplace central limit theorem. \square

Corollary 1. *The accuracy of a binary classification algorithm is asymptotically normal distributed with mean $\mu_{\text{ACC}} = p_N \mu_{R_{\text{TN}}} + p_P \mu_{R_{\text{TP}}}$ and variance $\sigma_{\text{ACC}}^2 = p_N^2 \sigma_{R_{\text{TN}}}^2 + p_P^2 \sigma_{R_{\text{TP}}}^2$, with $\sigma_{\text{ACC}}^2 \rightarrow \mu_{\text{ACC}}(1 - \mu_{\text{ACC}})/m$ as $m = |\text{P}| + |\text{N}| \rightarrow \infty$.*

Proof. This follows by writing the accuracy as a weighted sum $\text{ACC} = p_N R_{\text{TN}} + p_P R_{\text{TP}}$ of independent and asymptotically normal random variables. As a consequence, the accuracy is also asymptotically normal distributed with mean $\mu_{\text{ACC}} = p_N \mu_{R_{\text{TN}}} + p_P \mu_{R_{\text{TP}}}$. The independence of R_{TN} and R_{TP} (they refer to mutually exclusive subspaces) then implies that the variance is $\sigma_{\text{ACC}}^2 = p_N^2 \sigma_{R_{\text{TN}}}^2 + p_P^2 \sigma_{R_{\text{TP}}}^2$. From Lemma 3, $\sigma_{R_{\text{TN}}}^2 = \mu_{R_{\text{TN}}}(1 - \mu_{R_{\text{TN}}})/|\text{N}|$ and $\sigma_{R_{\text{TP}}}^2 = \mu_{R_{\text{TP}}}(1 - \mu_{R_{\text{TP}}})/|\text{P}|$. Therefore, σ_{ACC}^2 differs from $\mu_{\text{ACC}}(1 - \mu_{\text{ACC}})/m$ by a quantity of $O(1/m)$, with $m = |\text{P}| + |\text{N}|$ and $p_N = |\text{N}|/m$, $p_P = |\text{P}|/m$. This result was used in (10) to express the binomial confidence interval radius as $\delta(\text{ACC})_{\mathcal{N}} = z_p \sigma_{\text{ACC}}$. \square

Theorem 2. *If the output $\hat{y} \in [0, 1]$ of a binary classifier is perfectly calibrated (Guo et al., 2017), i.e. $\Pr([\hat{Y}] = Y | \hat{Y} = q) = q$ for all $q \in [0, 1]$, then the quantiles \hat{r}_p^l directly estimated by PIM from the validation errors $\varepsilon_l = y_l - \hat{y}_l$ are asymptotically consistent with the p -quantiles of the asymptotically normal distribution of the classification rates R_l .*

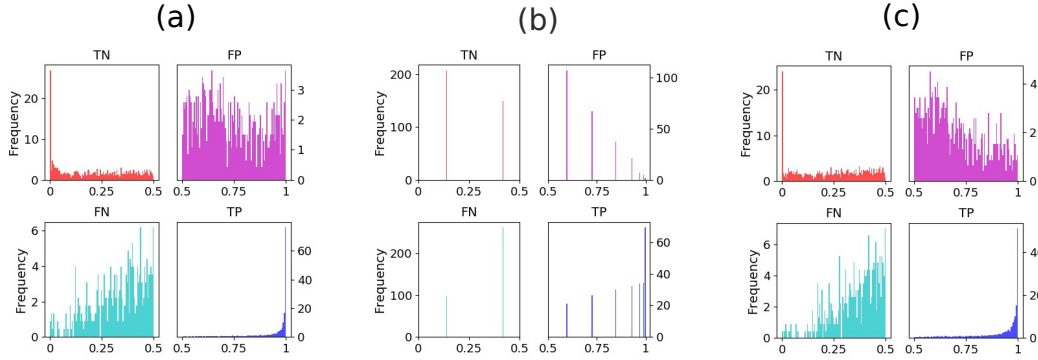


Figure S1: Confusion matrix shown as a normalized *distribution* of probability scores \hat{y} thrown by a classifier on the default test set of the *Adult* dataset: (a) original distributions (b) distributions after applying the Scaling-Binning calibrator (Kumar et al., 2019) (c) distributions after applying the Platt calibrator.

Note that perfect calibration is impossible in all practical settings. However, there are empirical approximations (calibration methods), some of them used in section S.3.4 below, which capture the essence of perfect calibration. A “well-calibrated” \hat{f} is understood here as model that, by designed, is calibrated or that has been calibrated properly after applying a calibration method. Before proceeding with the proof of Theorem 2, it helps to first visualize the meaning of the statement. In Figure S1, a plot of the empirical distribution of $\hat{Y} | Y$ is shown for a neural network with one hidden layer predicting on the test set of the *Adult* dataset in the UCI repository. It is noticed that, after applying a calibration method, the false predictions tend to cluster around the threshold $\tau = 0.5$, following a kind of Gaussian-like envelope. For true predictions, these cluster around the ground truth but displaying long tails depending on the calibration method. PIM is applied to find quantiles for the errors around the targets (for false predictions, the target is τ). The statement is then that, under certain conditions, these quantiles coincide with those of the distribution of the classification rates R_l of the corresponding $[\hat{Y}]$.

Proof. The proof proceeds by first showing that, if a classifier is perfectly calibrated, the quantiles of the predicted targets \hat{Y} are intimately connected with the expected value of the predictions. This is then used to pivot the errors $\varepsilon_l = y_l - \hat{y}_l$ with respect to the threshold τ when $s_l = F$ (i.e. $y_l = \tau$) and with respect to the ground truth when $s_l = T$ (i.e. $y_l = y$).

Using the notation of Definition 1, we seek an identity which links positive and negative predictions with true and false predictions. This is

$$[\hat{Y}]_\tau := \mathbb{1}(\hat{Y} > \tau) = \mathbb{1}(Y = 1) \mathbb{1}([\hat{Y}]_s = T) + \mathbb{1}(Y = 0) \mathbb{1}([\hat{Y}]_s = F),$$

which is valid for any threshold $\tau \in (0, 1)$. Taking expectation value on both sides,

$$\begin{aligned} \Pr(\hat{Y} > \tau) &= \Pr(Y = 1, [\hat{Y}]_s = T) + \Pr(Y = 0, [\hat{Y}]_s = F) \\ &= \Pr([\hat{Y}]_\tau = Y) = \int_0^1 \Pr([\hat{Y}]_\tau = Y | \hat{Y} = q_\tau(z)) \rho_{\hat{Y}}(z) dz, \end{aligned} \quad (12)$$

where $\rho_{\hat{Y}}$ is the probability density function of \hat{Y} associated to the cumulative distribution function $F_{\hat{Y}}(\hat{y}) = \int_0^{\hat{y}} \rho_{\hat{Y}}(\hat{y}') d\hat{y}'$, and q_τ belongs to a family of smooth functions $q_\tau : [0, 1] \rightarrow [0, 1]$ labeled by τ . If the classifier is perfectly calibrated,

$$\Pr([\hat{Y}]_\tau = Y | \hat{Y} = q_\tau(z)) = q_\tau(z), \quad \forall q_\tau(z) \in [0, 1].$$

Replacing this in (12) and denoting by $\langle q_\tau \rangle = \mathbb{E}_{\hat{Y}}(q_\tau)$ the expectation value of q_τ , we obtain

$$F_{\hat{Y}}(\tau) = \Pr(\hat{Y} \leq \tau) = 1 - \langle q_\tau \rangle. \quad (13)$$

Clearly, $\langle q_\tau \rangle \in (0, 1)$, so (13) states that τ coincides with the $(1 - \langle q_\tau \rangle)$ -quantile of $F_{\hat{Y}}$. For well-balanced datasets $p_N \simeq p_P \simeq 1/2$, the classifier will presumably learn to predict approximately the same amount of positive and negative predictions, so $\tau = 1/2$ will coincide with the median (= mean) of \hat{Y} , which is a special case of (13) for $\tau = \langle q_\tau \rangle = 1/2$

As in section 2.3, we are interested in the errors committed by the predictive model. In that section, these were measured with respect to the median of \hat{Y} (expected to coincide with Y). However, in the binary classification context, the median of \hat{Y} is not necessarily close to Y , as Fig. S1(c) suggests. The result implied by (13) then suggests that the errors $\varepsilon_l = y_l - \hat{y}_l$ committed by the predictive model be measured relative to the ground truth Y for $s_l = T$ and relative to τ for $s_l = F$. This leads to the quantile estimation problem for the error variable E_l as finding the \hat{r}_p^l such that the empirical error distribution functions evaluate to the confidence level p

$$F_l(\hat{r}_p^l) := \frac{1}{|v_l|} \sum_{i: [\hat{y}_i] = \bar{s}_l} \mathbb{1}(|\varepsilon_i^l| \leq \hat{r}_p^l) = p. \quad (14)$$

Such quantiles are estimated by PIM as an alternative to calculating the quantiles of \hat{Y} directly (similar to what was done in section 2.3). The reader is referred to Guo et al. (2017) for a proof that, for a perfectly calibrated classifier, the accuracy is locally distributed as the average confidence (here \hat{Y}). Since the classification rate R_l is the accuracy in the subspace indexed by l , this shows that the quantiles of R_l coincide with the corresponding quantiles of \hat{Y}_l . Furthermore, by Lemma 3, the R_l are asymptotically normally distributed. □

S.3.3 Uncertainty propagation

PIM uses four neurons u_l to measure confidence intervals $\hat{r}_p^l := \delta_p(R_l)$ for the classification rates R_l . Given the nature of classification $\delta_p(R_l) < 1$ with probability one. Knowing the value of p from the context, we can omit it from the δ subscript. It is then convenient to think of $\delta_p(R_l) := \delta R_l$ as a uncertainty that can be propagated to quantities dependent on $\{R_l\}$ using Taylor's theorem. This was done in (11) to go from $\text{ACC} = p_N R_{\text{TN}} + p_P R_{\text{TP}}$ to $\delta \text{ACC} = p_N \delta R_{\text{TN}} + p_P \delta R_{\text{TP}}$ by δ -differentiating both sides. The result is straightforward in this case because the relationship connecting the classification rates with the quantity of interest is linear. No error in the Taylor expansion is committed in this case. In this section, we would like to consider non-linear relationships and use uncertainty propagation techniques — as in the natural sciences — to find the associated uncertainties.

With \sim denoting the asymptotic value around which the classification rates cluster, it has been shown in Lemma 3 that

$$\begin{aligned} R_{\text{TP}} &= \frac{|\text{TP}|}{|\text{TP}| + |\text{FN}|} \sim \Pr([\hat{Y}] = 1 | Y = 1), \\ R_{\text{FN}} &= 1 - R_{\text{TP}} \sim \Pr([\hat{Y}] = 0 | Y = 1), \\ R_{\text{FP}} &= \frac{|\text{FP}|}{|\text{FP}| + |\text{TN}|} \sim \Pr([\hat{Y}] = 1 | Y = 0), \\ R_{\text{TN}} &= 1 - R_{\text{FP}} \sim \Pr([\hat{Y}] = 0 | Y = 0). \end{aligned} \quad (15)$$

It is of interest to estimate the uncertainty of other important rates, namely, positive predictive value (R_{TP}^* , a.k.a. precision), the false discovery rate (R_{FN}^*), the negative predictive value (R_{TN}^*), and the false omission rate (R_{FP}^*). These are obtained after interchanging the roles of predictions and ground truths. By symmetry,

$$\begin{aligned} R_{\text{TP}}^* &= \frac{|\text{TP}|}{|\text{TP}| + |\text{FP}|} \sim \Pr(Y = 1 | [\hat{Y}] = 1), \\ R_{\text{FN}}^* &= 1 - R_{\text{TP}}^* \sim \Pr(Y = 0 | [\hat{Y}] = 1), \\ R_{\text{TN}}^* &= \frac{|\text{TN}|}{|\text{TN}| + |\text{FN}|} \sim \Pr(Y = 0 | [\hat{Y}] = 0), \\ R_{\text{FP}}^* &= 1 - R_{\text{TN}}^* \sim \Pr(Y = 1 | [\hat{Y}] = 0). \end{aligned} \quad (16)$$

Taking the δR_l learned by PIM as independent variables (the neurons u_l are independent), it is assumed that the uncertainties of any smooth function g of $\{R_l\}$ can be approximated by Taylor's expansion:

$$\delta g(\{R_l\}) = \sum_q \left| \frac{\partial g}{\partial R_q} \right| \delta R_q + \frac{1}{2} \sum_{q \in F} \left| \frac{\partial^2 g}{\partial R_q^2} \right| (\delta R_q)^2 + \dots \quad (17)$$

When an *approximation* of δg is enough, only second order corrections are taken into account for false predictions, assuming they are more uncertain due to the (good enough) classification algorithm committing them less frequently. Now, by using Bayes' theorem, the asymptotic values in (15) and (16) can be connected as

$$\begin{aligned} \Pr(Y = \bar{v}_l \mid [\hat{Y}] = \bar{s}_l) &= \frac{\Pr([\hat{Y}] = \bar{s}_l \mid Y = \bar{v}_l) \Pr(Y = \bar{v}_l)}{\Pr([\hat{Y}] = \bar{s}_l)}, \\ &= \frac{\Pr([\hat{Y}] = \bar{s}_l \mid Y = \bar{v}_l) \Pr(Y = \bar{v}_l)}{\Pr([\hat{Y}] = \bar{s}_l \mid Y = 0) \Pr(Y = 0) + \Pr([\hat{Y}] = \bar{s}_l \mid Y = 1) \Pr(Y = 1)}. \end{aligned}$$

From this, it is easy to see that the most probable values of R_l^* and R_l are simply related. For instance,

$$\begin{aligned} R_{TP}^* &\sim \frac{R_{TP} p_P}{R_{TP} p_P + R_{FP} p_N}, \\ R_{TN}^* &\sim \frac{R_{TN} p_N}{R_{FN} p_P + R_{TN} p_N}. \end{aligned}$$

This relationships are examples of the g function above, so by (17), the uncertainties are related as

$$\begin{aligned} \delta R_{TP}^* &\sim \frac{p_N}{p_P} R_{TP}^{*2} \left[\frac{R_{FP}}{R_{TP}} \frac{\delta R_{TP}}{R_{TP}} + \frac{\delta R_{FP}}{R_{TP}} + \frac{p_N}{p_P} R_{TP}^* \left(\frac{\delta R_{FP}}{R_{TP}} \right)^2 \right], \\ \delta R_{TN}^* &\sim \frac{p_P}{p_N} R_{TN}^{*2} \left[\frac{R_{FN}}{R_{TN}} \frac{\delta R_{TN}}{R_{TN}} + \frac{\delta R_{FN}}{R_{TN}} + \frac{p_P}{p_N} R_{TN}^* \left(\frac{\delta R_{FN}}{R_{TN}} \right)^2 \right]. \end{aligned}$$

Uncertainties for other metrics derived from R_l , e.g the F1 score, can be obtained in a similar manner.

S.3.4 Effect of calibration

In the experiments of section S.3.1, no hyperparameter optimization is done. The only thing that is varied is the activation of the hidden layer (relu and tanh), and the calibration method for the predictions. Best results are reported.

It is noticed during experimentation that sometimes some of the estimates \hat{r}_p^l stay very close to their initial values (within a tolerance of 10^{-7}), for which NA is used when requesting their optimal values. This is often due to scarcity of data, since \hat{r}_p^l may not be updated for each of FN, FP, TN, TP within a mini-batch. For a classifier with relatively few false predictions, for instance, the optimal \hat{r}_p^F may not be found. Therefore, uncertainty on the rates of false predictions cannot be currently evaluated for small datasets.

This problem is not found for datasets like the *Adult* dataset (48,842 samples). Uncertainties estimated by PIM and propagated according to the technique described above are shown in Table S2. It is observed that calibrating the predictions leads most of the time to a decrease in the magnitude of the uncertainties, with a stabilization of the corresponding variance. However, for some rates the magnitude of the uncertainties still look too conservative. This is presumably due to the calibration method based on scaling not reaching calibrated-enough predictions, something typical according to the discussion in Kumar et al. (2019). The Scaling-Binary calibrator in Kumar et al. (2019) (whose effects are shown in Figure S1) is not considered in Table S2 since it does not give a continuous distribution of predictions, as required by PIM. Further research is desirable, combining the idea behind PIM with a suitable calibration method into one framework.

Table S2: Classification metrics with uncertainties learned by PIM in the Adult dataset: median \pm median of uncertainty (median absolute deviation of uncertainty) over an ensemble of 20 experiments. These are calculated with and without calibration. Temperature scaling is done with the code provided by Küppers et al. (2020)

CALIBRATION	R_{FP}	R_{TP}^*	ACC
UNCALIBRATED	0.38 ± 0.25 (0.03)	0.89 ± 0.09 (0.01)	0.85 ± 0.20 (0.02)
PLATT SCALING	0.41 ± 0.17 (0.02)	0.88 ± 0.07 (0.01)	0.85 ± 0.20 (0.00)
TEMPERATURE SCALING	0.38 ± 0.18 (0.01)	0.89 ± 0.07 (0.00)	0.85 ± 0.21 (0.01)